

Nucleation and growth of oxide islands during the initial-stage oxidation of (100)Cu-Pt alloys

Langli Luo, Yihong Kang, Judith C. Yang, and Guangwen Zhou

Citation: [Journal of Applied Physics](#) **117**, 065305 (2015); doi: 10.1063/1.4907801

View online: <http://dx.doi.org/10.1063/1.4907801>

View Table of Contents: <http://scitation.aip.org/content/aip/journal/jap/117/6?ver=pdfcov>

Published by the [AIP Publishing](#)

Articles you may be interested in

[Comparative study of the alloying effect on the initial oxidation of Cu-Au\(100\) and Cu-Pt\(100\)](#)

Appl. Phys. Lett. **104**, 121601 (2014); 10.1063/1.4870085

[Effect of gold composition on the orientations of oxide nuclei during the early stage oxidation of Cu-Au alloys](#)

J. Appl. Phys. **111**, 083533 (2012); 10.1063/1.4707929

[Composition effects on the early-stage oxidation kinetics of \(001\) Cu-Au alloys](#)

J. Appl. Phys. **101**, 033521 (2007); 10.1063/1.2433714

[Effects of surface topology on the formation of oxide islands on Cu surfaces](#)

J. Appl. Phys. **97**, 063509 (2005); 10.1063/1.1861147



[From nucleation to coalescence of Cu₂O islands during in situ oxidation of Cu\(001\)](#)

Appl. Phys. Lett. **81**, 241 (2002); 10.1063/1.1492007



AIP | Journal of Applied Physics

Meet The New Deputy Editors

	Christian Brosseau		Laurie McNeil		Simon Phillpot
---	---------------------------	---	----------------------	---	-----------------------

Nucleation and growth of oxide islands during the initial-stage oxidation of (100)Cu-Pt alloys

Langli Luo,¹ Yihong Kang,² Judith C. Yang,³ and Guangwen Zhou^{1,a)}

¹Department of Mechanical Engineering and Multidisciplinary Program in Materials Science and Engineering, State University of New York, Binghamton, New York 13902, USA

²Department of Mechanical Engineering and Materials Science, University of Pittsburgh, Pittsburgh, Pennsylvania 15261, USA

³Department of Chemical and Petroleum Engineering, University of Pittsburgh, Pittsburgh, Pennsylvania 15261, USA and Department of Physics, University of Pittsburgh, Pittsburgh, Pennsylvania 15261, USA

(Received 5 November 2014; accepted 28 January 2015; published online 11 February 2015)

The initial-stage oxidation of (100) Cu-Pt alloys has been examined by *in situ* environmental transmission electron microscopy and *ex situ* atomic force microscopy (AFM). It is shown that the oxidation proceeds via the nucleation and growth of Cu₂O islands that show dependence on the alloy composition and oxidation temperature. The kinetic measurements on the oxide nucleation reveal that both the nucleation density and surface coverage of Cu₂O islands can be promoted by alloying more Pt in the Cu-Pt alloys. Increasing the oxidation temperature above 700 °C results in the growth of large Cu₂O islands that transits to a dendritic growth morphology. The *ex situ* AFM studies reveal that the nucleation of oxide islands can occur on surface terraces and the subsequent oxide growth depletes local terrace Cu atoms that results in the formation of surface pits. © 2015 AIP Publishing LLC. [<http://dx.doi.org/10.1063/1.4907801>]

I. INTRODUCTION

Understanding the oxidation mechanism of alloys is intrinsically critical for the development of oxidation-resistant alloys. Cu-Pt alloys can be used as ideal model systems for understanding the effect of alloying on the oxidation mechanism since Cu as the major element is oxidized exclusively leaving the non-oxidizable metal Pt enriched in the alloy. Oxygen is less soluble in Cu-Pt alloy comparing with Cu-Au or Cu-Pd alloys, and the enriched Pt diffuses slowly in the alloy phase that effectively reduces the rate of oxidation.¹ Besides, Cu-Pt alloys have attracted growing interest as heterogeneous catalysts for the water-gas shift reaction in fuel cells² and nitrate reduction in water remediation³ as well as next generation memory devices.⁴ Especially, the surface oxidation of Cu-Pt and Cu-Au alloys as package materials largely affects the reliability of microelectronic devices when multiple metals are incorporated together in an ever-shrinking size.^{5,6}

As the sizes of the material systems approach the nanoscale, it is important to understand their environmental stability at the nanometer or atomic scale, which is much smaller than the regime of traditional oxidation/corrosion studies that typically focus on the growth of a continuous, macroscopically thick oxide layer. For bulk metals or alloys such as those used as structural materials, the oxide scale formed on the surface can grow to tens of microns without significantly affecting its mechanical properties. In contrast, with an increased interconnect density and a decrease in the dimensions of interconnects, the problem of environmental stability of interconnects (e.g., Cu and Cu based alloys) at

the nanometer scale becomes much more critical. The formation of a just few nanometer-thick oxide overlayer can largely affect the mechanical and electrical properties of the Cu interconnects as their size is scaling down into nanometer range. The use of Cu nanoparticles in heterogeneous catalysis is another example where the surface stability at the nanometer scale is a critical issue, which may lead to significant change in the catalytic property by oxidizing just a few layers of Cu atoms at the surfaces. Though scanning tunneling microscopy (STM) has provided fruitful information of metal-gas interactions in atomic scale under ultra-high vacuum condition, it lacks information under realistic conditions and has poor temporal resolution for *in situ* studies. Environmental transmission electron microscopy (E-TEM) provides both high spatial and temporal resolution for obtaining real-time information under near technology-relevant conditions for bridging the information gap between the knowledge obtained from surface science approaches that mainly focus on oxygen adsorption of up to one monolayer and that of the traditional oxidation studies of the growth of continuous, macroscopically thick oxide layer.

Generally, oxidation of metals starts typically with oxygen chemisorption induced two-dimensional (2D) surface structures followed by nucleation and growth of oxide films.⁷ These oxide films may grow on or embed into the metal substrate depending on composition and crystal structure of the surface as well as oxidation conditions. Before the metal surface is fully covered with a continuous oxide layer, the growth of three-dimensional (3D) oxide islands is often observed for the oxidation of pure metals such as Cu, Ni, Fe, Mo,^{8–15} and alloys such as Cu-Ni, Cu-Mn, Pd-Zn, and Cu-Au.^{16–21} Alloying Cu with Au can promote the nucleation of Cu₂O islands but reduce the growth rate of the oxide islands.^{21,22} In addition to its effect on the initial oxidation

^{a)}Author to whom correspondence should be addressed. Electronic mail: gzhou@binghamton.edu

kinetics, alloying Cu with Au can also affect the oxide growth morphology. For instance, the oxidation of (100) Cu-Au at 600 °C results in the formation of Cu₂O islands that initially have a compact shape followed by transition to a dendritic morphology owing to the variation in the oxide growth rate along the perimeter of the oxide island induced by the non-uniform partition of Au atoms in the surrounding Cu-Au alloy.²⁰ Alloying Cu with Pt provides additional insight into understanding the effect of alloying on the modification of the oxidation behaviour from the pure metal. In a comparative study of the oxidation of (100)Cu-Au and (100)Cu-Pt, it has been shown that Cu₂O islands formed on the (100)Cu-Au surface deeply embed into the Cu-Au substrate while Cu₂O islands formed on the (100)Cu-Pt surface highly protrude above the Cu-Pt substrate.²³ This difference in the oxide growth morphology is attributed to the different mobilities of Au and Pt in Cu, where the high mobility of Au in Cu results in fast partition of Au in the surrounding Cu-Au alloy while the low mobility of Pt in Cu results in trapped Pt at the oxide/alloy interface.²³

Herein, we extend the earlier work by performing a detailed study on the effect of alloying Cu with Pt on the nucleation and growth kinetics of Cu₂O islands during the initial-stage oxidation of the (100)Cu-Pt alloys. With the use of the *in-situ* environmental TEM to monitor the nucleation and growth of oxide islands, we study the initial-stage oxidation of the Cu-Pt solid solutions with the composition of 5 at. %Pt and 10 at. %Pt at the temperature varying from 350 °C to 800 °C. *Ex-situ* atomic force microscopy (AFM) is also employed to unravel further details on the nucleation and growth mechanism of oxide islands.

II. EXPERIMENTAL

The oxidation experiments were performed in an environmental TEM (modified from JEL200CX) capable of observation of oxidation in real time. Electron transparent Cu-Pt(100) thin films with $\sim 700 \text{ \AA}$ thickness were grown on NaCl(100) by co-deposition in an UHV e-beam evaporation system. The alloy films were then removed from the substrate by floatation in deionized water and mounted on a TEM specimen holder. A leak valve attached to the TEM column permits introduction of gases directly into the TEM with a controlled oxygen gas pressure (p_{O_2}). The sample can be locally heated in the TEM column with controlled temperature. Before oxidation experiments, native oxide can be removed by annealing in the TEM chamber at 750 °C under vacuum condition^{24,25} or *in situ* annealing under H₂ gas at pressure $\sim 10^{-5}$ Torr and 350 °C, resulting in a clean surface. The sample cleanliness can be checked by electron diffraction. Oxygen gas of 99.999% purity was then admitted into the column of the microscope through the leak valve to oxidize cleaned alloy films at a constant temperature and oxygen pressure p_{O_2} (the oxygen pressure used in this paper is $p_{\text{O}_2} = 5 \times 10^{-4}$ Torr if not specified). *In situ* TEM observations of the oxidation process were made in planar views. Careful oxidation experiments with and without electron beam irradiation were conducted and similar growth morphologies, and island sizes were observed in both cases. In

most cases, the electron beam was on only when taking TEM images to further minimize any possible electron beam effect. Surface topologies of the post-oxidized samples were characterized by a Veeco[®] Dimension V scanning probe microscopy (SPM) system. To minimize surface contamination and further oxidation resulting from long exposure to air, *ex-situ* AFM experiments were performed immediately after the sample was taken out from the TEM apparatus. *Ex-situ* AFM experiments of as-annealed Cu samples (without oxidation) indicate that the surface remained flat without noticeable oxide island formation, suggesting that the subsequent air exposure did not cause appreciable changes to the surface topology of the sample oxidized in the TEM apparatus.²⁶

III. RESULTS AND DISCUSSION

A. Composition effect on the nucleation and growth of oxide islands

The nucleation of an oxide island on the alloy surface requires overcoming an energy barrier associated with a critical island size.²⁷ The main contributions to the energy barrier are volume free energy, surface/interface energy, and interfacial strain energy that depends on the lattice mismatch between the oxide and the alloy substrate. According to Vegard's law, a linear relation exists between the lattice constant of an alloy and the concentrations of the constituent elements. Both Cu and Pt are face-centred cubic with the lattice constants of 3.61 Å and 3.92 Å, respectively. Therefore, the lattice constant of the Cu-Pt alloy increases with increasing Pt content in the alloy, which may modify the oxide/alloy lattice mismatch (the interfacial strain energy) and thus the nucleation kinetics of the oxide islands. To test the effect of the alloy composition on the oxide nucleation, we examined the oxidation of two alloy compositions, Cu-5 at. % Pt and Cu-10 at. % Pt, under the same oxidation condition ($T = 350 \text{ °C}$ and $p_{\text{O}_2} = 5 \times 10^{-4}$ Torr). Our *in situ* TEM observations indicate that an incubation period is needed, for both alloys, before the appearance of visible oxide nuclei on the alloy surface after oxygen gas was introduced into the TEM. A longer incubation time was needed to nucleate oxide islands for the Cu-10 at. % Pt.

Figs. 1(a)–1(d) present a series of time-resolved bright-field TEM images during oxidation of the Cu-5 at. % Pt(100) thin film at $T = 350 \text{ °C}$ and $p_{\text{O}_2} = 5 \times 10^{-4}$ Torr. Fig. 1(a) is a representative TEM image of the sample after being cleaned by annealing in H₂ at 350 °C, where the contrast variation across the film is caused by the non-uniform thickness of the Cu-Pt alloy film. Only one set of electron diffraction pattern corresponding to the Cu-Pt solid solution can be obtained from the cleaned sample, indicating that the native oxide was completely removed and no ordered Cu-Pt phases developed in the Cu-Pt film. Oxygen gas was then introduced into the TEM column to oxidize the sample at $T = 350 \text{ °C}$ and $p_{\text{O}_2} = 5 \times 10^{-4}$ Torr. After 5 min of the oxygen exposure, a few oxide islands with slightly darker contrast became visible on the alloy thin film, as indicated by arrows in Fig. 1(b). Because of the small thickness of these oxide islands, they showed weak contrast and were barely differentiated from the non-uniform thickness contrast of the Cu-Pt

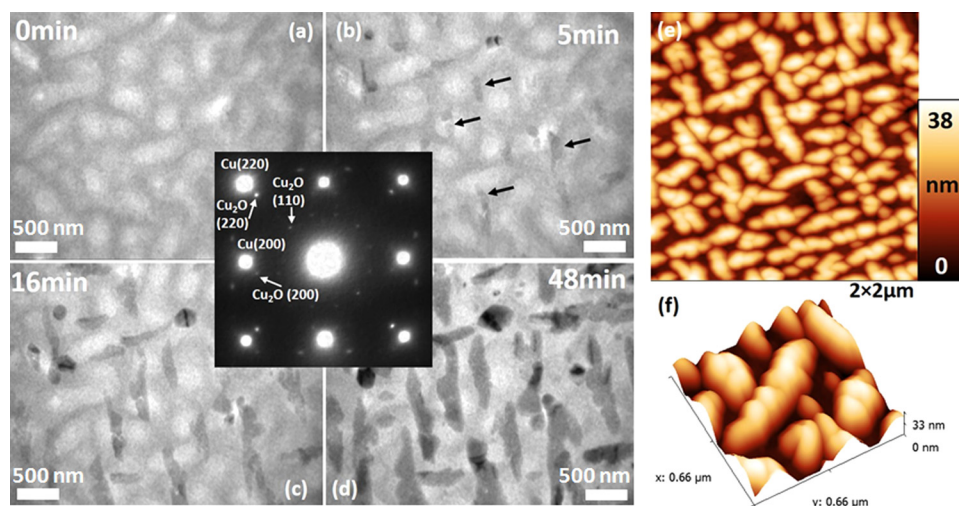


FIG. 1. (a)–(d) Time-resolved bright-field TEM images of surface oxidation of the Cu-5 at. %Pt(100) alloy thin film at $T = 350^\circ\text{C}$ and $p\text{O}_2 = 5 \times 10^{-4}\text{Torr}$. Inset is an SAED pattern of the oxidized surface showing epitaxially grown Cu_2O oxide islands. (e) AFM height image of the typical surface profile of oxide islands, and (f) the corresponding 3D AFM image.

alloy film. With continued oxidation, these initially compact oxide islands became progressively elongated as they grew larger in size as shown in Figs. 1(c) and 1(d). The elongation directions of the islands are along the [110] or $[\bar{1}10]$ directions of the substrate. As seen in Figs. 1(c) and 1(d), the oxide islands gained more mass contrast with the continued oxygen exposure, indicating that the oxide islands grew in three dimensions that resulted in thickness increase. The inset is a selected area electron diffraction (SAED) pattern obtained from the oxidized film, which can be indexed as two sets of diffraction patterns: One is associated with the solid-solution Cu-Pt substrate, and the other weaker one with the oxide islands that have Cu_2O phase with a cube-on-cube epitaxial relationship with Cu-Pt substrate. The absence of

other diffraction spots indicates that Cu is selectively oxidized to form Cu_2O , for which Pt is segregated into the alloy.

Fig. 1(e) is an *ex situ* AFM image of the Cu-Pt(100) thin film after one-hour oxidation at 350°C and $p\text{O}_2 = 5 \times 10^{-4}\text{Torr}$. It further confirms that the oxide islands have an elongated shape. The high surface coverage ($\sim 78\%$) of the oxide results in interpenetrating elongated oxide islands. The 3D surface profile of the AFM image as shown in Fig. 1(f) indicates that these Cu_2O islands have a maximum height of 38 nm and a length/width aspect ratio up to $\sim 5:1$ with the length up to 500 nm. It can be seen in Figs. 1(e) and 1(f) that the elongated islands show multiple segments, suggesting that the elongated islands are formed by the coalescence of smaller

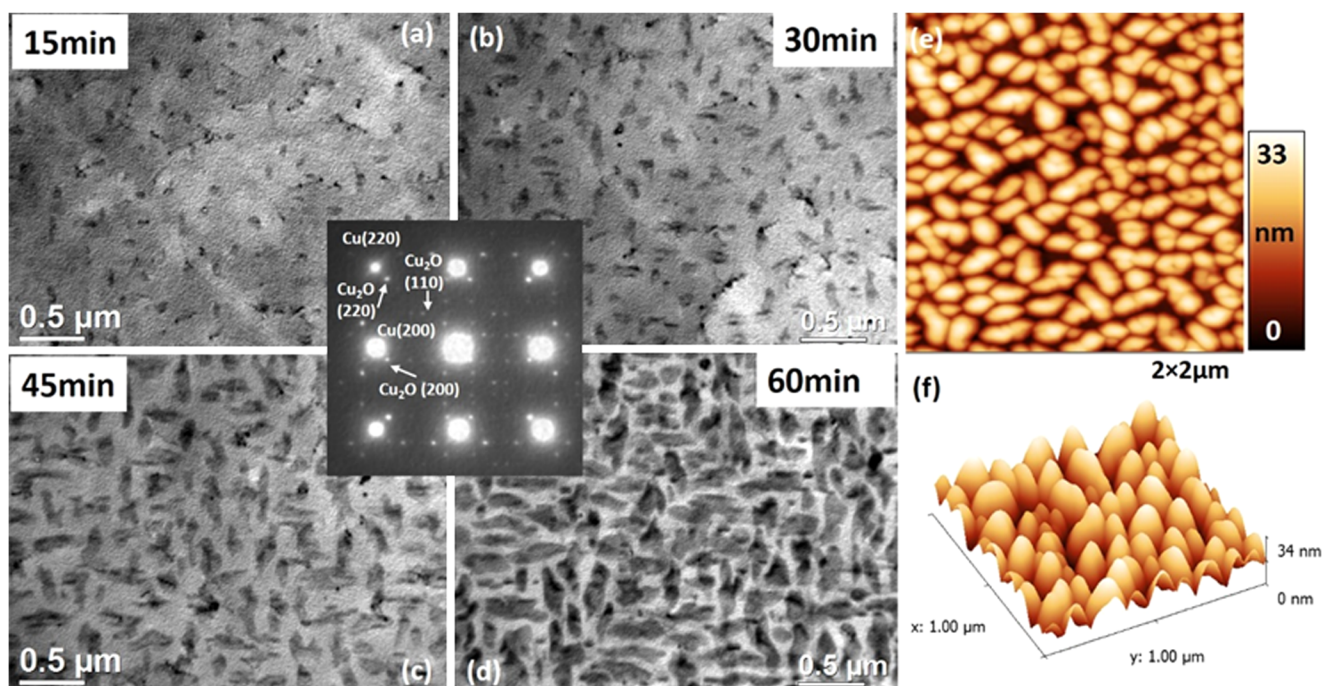


FIG. 2. (a)–(d) Time-resolved bright-field TEM images of surface oxidation of the Cu-10 at. %Pt(100) alloy thin film at $T = 350^\circ\text{C}$ and $p\text{O}_2 = 5 \times 10^{-4}\text{Torr}$. Inset is an SAED pattern of the oxidized surface showing epitaxially grown Cu_2O islands. (e) AFM height image of the typical surface profile of the oxide islands and (f) corresponding 3D AFM image.

round/oval shaped oxide islands. It can be seen from the AFM images that there are some smaller and uncoalesced oxide islands present on the surface after 1 h oxidation. The AFM observations also show that the oxidation results in significantly increased surface roughness compared to the as-annealed Cu surfaces.²⁶

Figs. 2(a)–2(d) are a time sequence of bright-field TEM images showing the nucleation and growth of oxide islands on a Cu-10 at. %Pt(100) thin film during the oxidation at $T = 350^\circ\text{C}$ and $p\text{O}_2 = 5 \times 10^{-4}$ Torr for 1 h. Oxide nuclei were barely visible initially due to their weak TEM image contrast. After the lapse of ~ 15 min of the oxidation, oxide islands can be clearly identified (Fig. 2(a)), and there was barely new oxide island formation as the oxidation continued. The oxide islands had a narrow size distribution and a smaller average size (< 50 nm) compared with that on the Cu-5 at. %Pt(100) sample. During the growth stage, the oxide islands developed into an elongated morphology with the elongation directions along the [110] or $[\bar{1}\bar{1}0]$ directions of the substrate. Inset in Fig. 2 is an SAED pattern obtained from the oxidized alloy, which can be indexed well with the Cu-Pt solid solution and the Cu_2O structure. The electron diffraction analysis indicates that Cu is selectively oxidized to Cu_2O , similar as the oxidation of the Cu-5 at. %Pt(100) sample. Figs. 2(e) and 2(f) are *ex situ* AFM images of the oxidized sample, which show that the maximum height of the oxide islands is ~ 34 nm. The length/width aspect ratio of the oxide islands is less than 2:1, and the length of oxide islands ranges from ~ 100 nm to 200 nm, which are both smaller than the oxide islands on the surface of the Cu-5 at. %Pt(100) sample. Meanwhile, while the average size of oxide islands decreased, the nucleation density of oxide islands increased significantly, resulting in an increasing oxide coverage of $\sim 90\%$ for the oxidation of Cu-10 at. %Pt(100) compared to Cu-5 at. %Pt(100) under the same oxidation condition. From the electron diffraction patterns shown in Figs. 1 and 2, one can note that the oxide islands had a cube-on-cube epitaxial relation with the Cu-Pt substrate for both the alloy compositions.

From the *in situ* TEM and *ex situ* AFM observations, we can find that oxidation of the Cu-Pt alloys at 350°C produced a high surface coverage of small oxide islands with sizes ranging from 50 to 500 nm and an average height ~ 35 nm protruding above the alloy surface. It should be noted that the total island thickness can be larger than 35 nm since the oxide islands can also grow into the substrate, i.e., the oxide/metal interface gradually migrates into the substrate as the oxidation continues. The oxidation of the Cu-10 at. %Pt sample generated a larger nucleation density but a smaller size of oxide islands compared to the Cu-5 at. %Pt sample. Besides, the oxide islands on the surface of the lower Pt content alloy showed more pronounced elongation growth. According to Vegard's law, the lattice parameter of the Cu-Pt alloy increases with increasing Pt concentration for the solid solution Cu-Pt alloy. The decrease of lattice mismatch between Cu_2O ($a = 4.27 \text{ \AA}$) and Cu-Pt ($3.61 \text{ \AA} < a < 3.92 \text{ \AA}$) can lower the activation energy for oxide nucleation,²¹ leading to an enhanced nucleation density by increasing the Pt content in the alloy. This effect of Pt

alloying with Cu on the nucleation and growth of Cu_2O islands is similar as the oxidation of Cu-Au alloys, in which the effect of Au is to enhance the nucleation density of oxide islands but slow down their growth rate.²⁸

The above observations also reveal that the tendency for the elongation of the oxide islands depends on the alloy composition. The alloy with the higher Pt content shows less pronounced one dimensional oxide growth. The growth morphology of the oxide islands can be controlled by an interplay of thermodynamics and kinetics,^{29–31} where the energy minimization in the oxide island drives the shape transition from the initially compact shape to the elongated morphology at a critical island size while the sufficient surface mobility of oxygen atoms allows for the oxide growth with the equilibrium island shape. The minimum energy path for oxygen atoms hopping between fcc hollow sites is along the $\langle 110 \rangle$ directions with an energy barrier of ~ 0.71 – 0.75 eV.^{32,33} Due to the low Pt concentration in the Cu-5 at. %Pt(100) thin film, the favorable diffusion path of oxygen atoms is along the $\langle 110 \rangle$ directions, which therefore facilitates the elongation of the oxide islands along these directions. However, with increasing Pt concentration, the oxygen surface diffusion is promoted since Pt(100) has a smaller diffusion barrier ~ 0.51 eV for oxygen atoms.³⁴ The solid solution phase of the Cu-Pt alloy (Pt concentration less than 15 at. %) has Cu and Pt atoms randomly distributed on the equivalent sites of the fcc structure. Then, the oxygen surface diffusion is prompted in all possible directions, resulting in less-pronounced elongation growth of oxide islands for a higher Pt concentration in the alloy.

B. Temperature effect on the nucleation and growth of oxide islands

We have investigated the effect of oxidation temperature on the nucleation density and growth morphology of oxide islands on Cu-5 at. %Pt(100). Figs. 3(a), 3(b), and 3(c) show the typical morphologies of the oxide islands for the oxidation at 500°C , 600°C , and 700°C , respectively, where all oxide islands have a Cu_2O phase and have regular faceted shapes (triangular, square, or trapezoid shapes). With increasing oxidation temperature, the lateral size of the oxide islands increased from sub-micron to $2 \mu\text{m}$ and number density of oxide islands (i.e., the number of oxide islands per unit area, μm^2 , which can be directly measured from the TEM images) decreased dramatically. The apparent activation energy for the nucleation of oxide islands can be deduced from the dependence of the island density on oxidation temperature. The nucleation of an oxide island requires the capture of oxygen atoms, i.e., there is an active zone of oxygen capture around each oxide island. The radius of this capture zone is proportional to the oxygen surface diffusion rate and the probability of a nucleation event is proportional to the fraction of available surface area outside these zones of oxygen capture. Due to the higher surface mobility of oxygen atoms at a higher temperature, the radius of oxygen capture zone increases with temperature and the attachment of oxygen to existing oxide islands is more favorable than nucleation of new oxide islands. Therefore, the density of

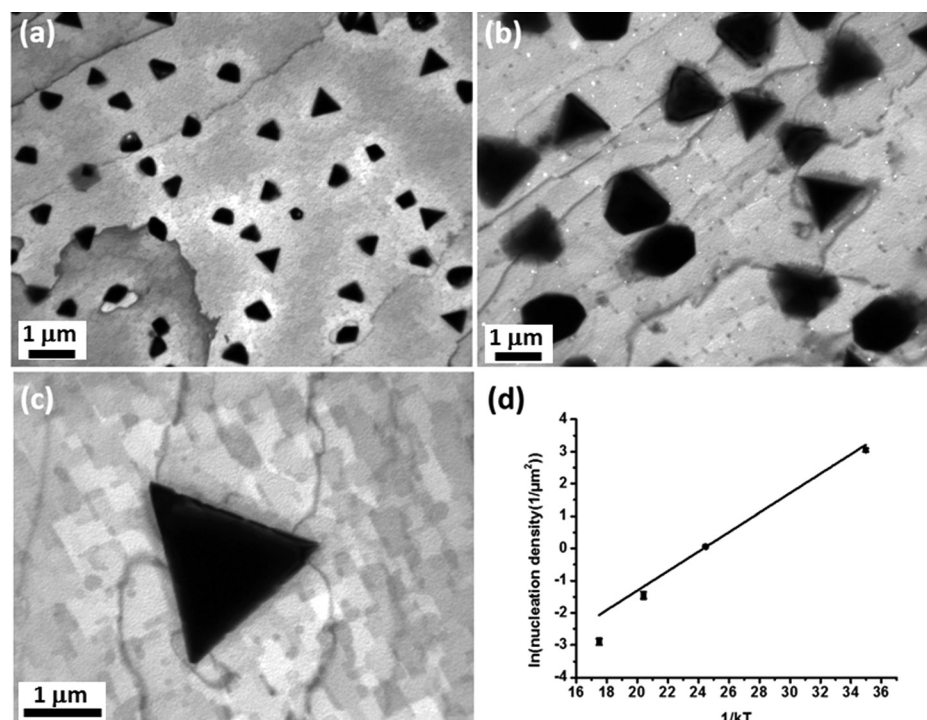


FIG. 3. Bright-field TEM images of surface oxidation of the Cu-5 at. %Pt(100) alloy thin film at (a) 500 °C, (b) 600 °C, and (c) 700 °C. (d) Plot of nucleation density vs. $1/kT$ representing the Arrhenius dependence of the nucleation density of oxide islands on temperature. The nucleation barrier of the oxide islands can be obtained from the slope of the plot.

oxide islands follows an Arrhenius relationship $N_s \sim e^{-E_a/kT}$ with oxidation temperature,³⁵ where k is Boltzmann's constant, T is the oxidation temperature, and E_a is the activation energy for oxide nucleation. By measuring the island density at different oxidation temperatures, the activation energy, E_a , can be determined. Fig. 3(d) shows the Arrhenius dependence of nucleation density on temperature plotted for the oxidation at the temperature ranging from 350 °C to 700 °C for the Cu-5 at. %Pt(100). E_a for the oxide nucleation is determined to be 0.3 ± 0.15 eV by the slope of the plot in Fig. 3(d). Note that the nucleation activation energy depends on the energies of nucleation, dissociation of molecular oxygen, absorption and/or desorption of oxygen, and not necessarily only on the oxygen surface diffusion barrier. Therefore, it is the overall energy required for oxide island nucleation without differentiating the different elementary steps involved. A qualitative comparison can be made between the oxidation of Cu-5 at. %Pt(100) and Cu(100). The oxide nucleation barrier for the oxidation of Cu(100) was determined to be 1.4 ± 0.2 eV,³⁵ which is larger than the nucleation of oxide islands on Cu-5 at. %Pt(100) shown here. This indicates that the effect of alloying Cu with Pt promotes the nucleation of oxide islands. Pt is known to be more reactive toward O_2 dissociation than Cu.^{36,37} Therefore, the increase in the content of Pt also promotes the dissociation of oxygen molecules and thus contributes to the reduction in the oxide nucleation barrier in addition to the aforementioned effect of the decrease in the lattice mismatch that facilitate epitaxial nucleation of oxide islands by alloying Cu with more Pt.

After determining the effect of temperature on the nucleation kinetics of oxide islands, we then focus on the growth of individual oxide islands during the oxidation. Figs. 4(a)–4(f) show a sequence of time-resolved bright-field TEM images revealing the entire process from the nucleation

of a single oxide island to its growth during the oxidation of Cu-5 at. %Pt(100) at $T=700$ °C and $pO_2=5 \times 10^{-4}$ Torr. The time when a visible oxide island emerged was defined as the start of the oxidation (i.e., 0 s) for measuring the growth rate of the oxide island. Actually, an incubation period was required which can last from a few minutes to tens of minutes depending on oxidation temperature, oxygen pressure, and the alloy composition. As seen in Fig. 4(a), a barely visible dark spot appeared first in the view, as indicated by the arrow. Once a stable oxide nucleus was formed, it grew very fast. As shown in Figs. 4(b) and 4(c), the oxide island grew into several hundred nanometres laterally and developed to a triangular shape within a few seconds. After the edge of triangular island reached ~ 1 μm , the lateral growth rate of the oxide island dropped quickly. By measuring the cross-sectional area of the oxide island at the different oxidation times, a linear relation is plotted in Fig. 4(g). This quasi-linear growth rate of the oxide island is similar as the oxidation of pure Cu, which has been quantified by a 3D island growth model with oxygen surface diffusion as the rate-limiting process.³⁸ The linear growth of the oxide island suggests that the growth of oxide islands during the oxidation of the Cu-Pt(100) surface is still dominated by oxygen surface diffusion. The AFM height image in Fig. 4(h) shows a single oxide island grown on the same surface of the oxidized Cu-5 at. %Pt(100) sample. The surface profile analysis indicates that the oxide island has a height of ~ 560 nm protruding above the Cu-Pt surface, which further confirms the 3D growth of the oxide island.

Alloying with noble metals such as Au can cause a notable morphology change in the surface oxide. A transition from compact to dendritic morphology of oxide islands has been observed during the oxidation of the Cu-Au alloys,²⁰ which indicates a transition in the rate-limiting factor in the oxide growth from oxygen surface diffusion to the diffusion

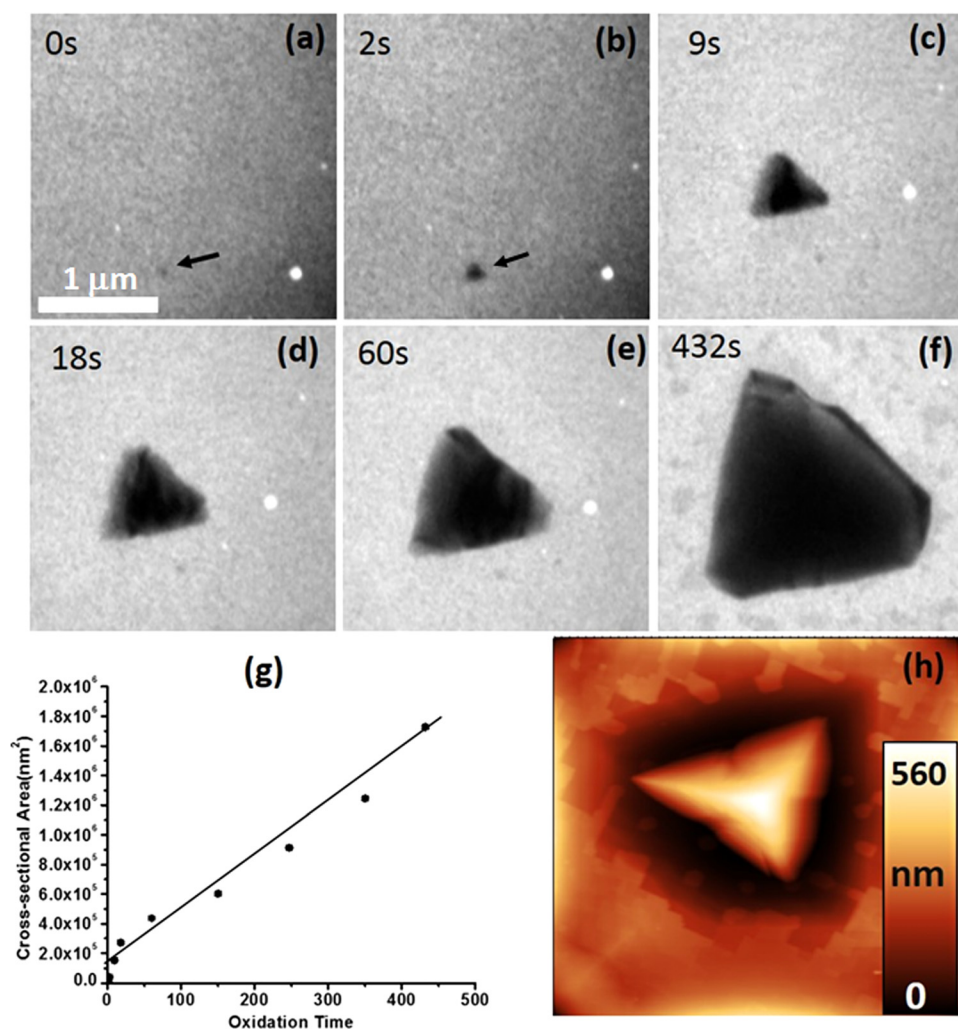


FIG. 4. (a)–(f) A sequence of the growth of a single oxide island on the Cu-5 at. %Pt(100) surface at 700 °C; (g) Cross-sectional area of the oxide island vs. oxidation time. (f) AFM height image of the typical surface profile of a single oxide island formed at 700 °C.

of copper through the increasingly gold-rich regions adjacent to the oxide island. Dendritic growth of oxide islands was observed here during the oxidation of the Cu-10 at. %Pt(100) when the oxidation temperature was above 700 °C. Fig. 5 shows a time sequence of *in situ* TEM images revealing how the morphology of a typical triangular Cu_2O island evolved during the oxidation of the Cu-10 at. %Pt(100) surface at 700 °C. The oxide island had a triangular shape and maintained this shape during the initial ~ 6 min of its growth. Thereafter, it began to branch at one corner of the triangular oxide island by protruding from the edges along the arrow directions shown in Fig. 5(d). Meanwhile, the sharp edges and corners of the triangular oxide islands became multifaceted owing to the branching.

Increasing oxidation temperature can promote the dendritic oxide growth (i.e., branching), and Fig. 6 shows the typical morphology of the dendritic growth of oxide islands formed from the oxidation of Cu-10 at. %Pt(100) at 800 °C. Fully developed dendritic oxide spread across the surface with branches and sub-branches. The areas adjacent to these dendritic branches shows highly dark contrast in the bright-field TEM imaging mode, indicating Pt is enriched in these areas. The selected area electron diffraction patterns shown in the lower panel of Fig. 6 were obtained from the different regions around the dendritic oxide. Diffraction pattern 1

corresponds to region 1 indicated in Fig. 6(a), where Pt is highly enriched, and develops into the ordered Cu_3Pt phase at room temperature. The regions far away from the oxide growth front, such as region 2, have the FCC structure as

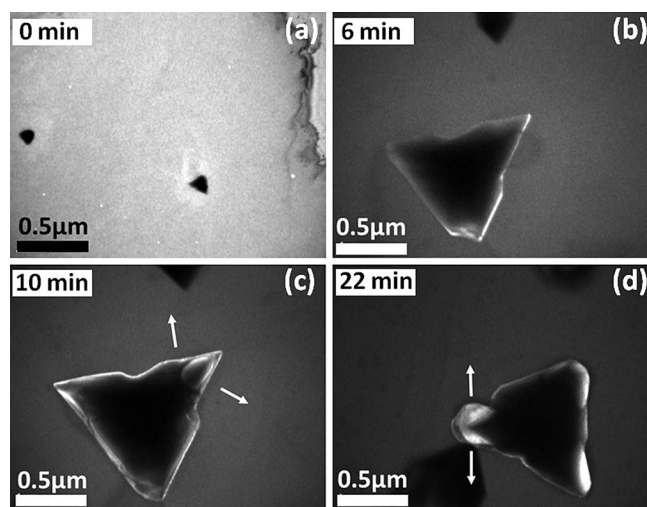


FIG. 5. Time-resolved bright-field TEM images of surface oxidation of the Cu-5 at. %Pt(100) alloy thin film at 700 °C showing a shape transition during the growth of the oxide island.

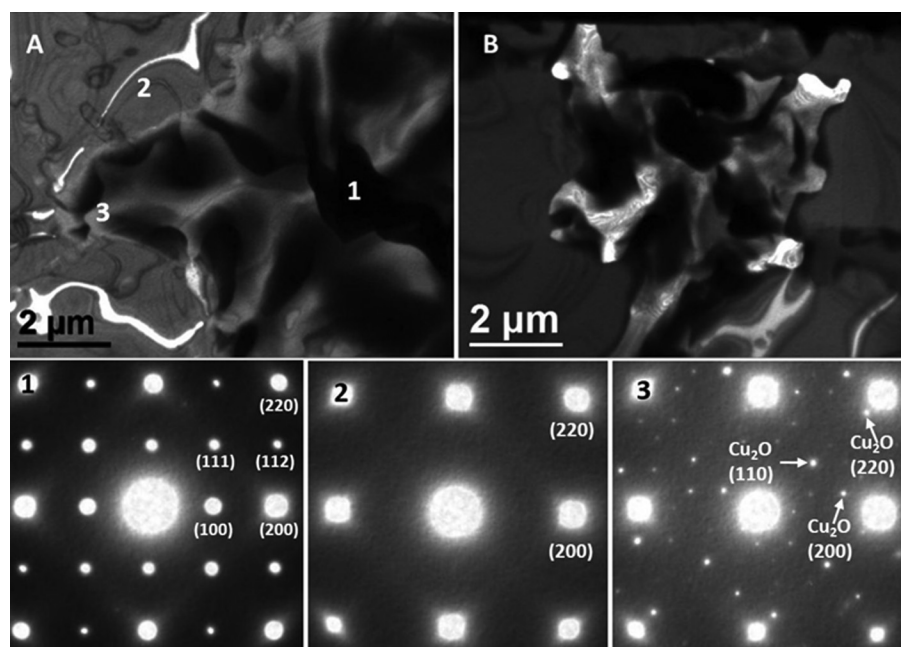


FIG. 6. (a) and (b) Typical dendritic growth of the oxide film on the Cu-5 at. %Pt(100) alloy thin film at 800°C and the SAED patterns shown in lower panel are obtained from regions 1, 2, and 3 marked in (a).

observed prior to oxidation. The diffraction pattern obtained from region 3 indicates that the oxide island is single crystal that nucleates in an epitaxial orientation relationship with the substrate. The $L1_2$ -Cu₃Pt phase was not observed for Cu-10 at. %(100) before oxidation, but was formed after the oxide growth. This observation indicates that similar as the Cu-Au alloy,²⁰ the oxidation of Cu-Pt alloys is accompanied by the rejection of Pt atoms from the growing front, leading to the formation of Pt-rich zones in the alloy adjacent to the oxide island. However, the temperature required for such fast Pt partition is 100°C higher than the Cu-Au oxidation because of the slower mobility of Pt in Cu than that of Au in Cu.^{39,40} Thermodynamically, Cu tends to oxidize more readily than Pt in terms of forming a stable oxide phase from their respective pure metals. In this case, depending on the oxidation conditions (oxygen pressure, temperature), either one or both components of the alloy will oxidize. Therefore, despite the fact that Cu is less reactive toward O₂ dissociation than Pt, Cu is selectively oxidized to form Cu₂O while Pt still remains its metallic state under the oxidation conditions employed in our study. The gradual depletion of Cu in the alloy results in the enrichment of Pt in the surrounding alloy and slows down the oxide growth adjacent to the Pt-rich zones, which leads to the transition in Cu₂O growth from the initially compact shape to the branched morphology.

C. Effect of surface defects on the nucleation and growth of oxide islands

While the plan-view *in situ* TEM imaging provided detailed information on the nucleation kinetics and growth morphologies of oxide islands, the effect of surface defects such as surface steps on the oxide nucleation and growth cannot be elucidated since it is not easy to discern surface steps in this imaging mode. In order to get this information a Cu-5 at. %Pt(100) sample slightly oxidized at 400°C was examined further by *ex situ* AFM. Fig. 7(a) shows a representative AFM height image of the surface of the oxidized

Cu-5 at. %Pt(100), and Fig. 7(b) is the height profiles drawn across an oxide island and the step edge as marked in Fig. 7(a). The alloy surface shows flat terrace regions and well-defined straight steps with a step height of 1 nm. The white round/oval dots are oxide islands with an average lateral size of 15.4 nm and a height ranges from 2 to 5 nm. While a few oxide islands are observed to sit right adjacent to the edge of the straight steps, more oxide islands are actually nucleated at the terrace region accompanied with shallow pits (less than 2 nm deep). The edges of these pits are smoothly curved and show a distinguishably different morphology from the straight step edges, which serves as a clear indication that the nucleation of these oxide islands occurred on the terrace and formation of the shallow pits was induced by the growth of the oxide islands with the consumption of nearby terrace atoms, leaving pits adjacent to the growing oxide islands. The observed homogenous nucleation of oxide islands (i.e., the oxide nuclei form not exclusively at surface defect sites) during the oxidation of the Cu-5 at. %Pt(100) is also in accordance with our previous observations of the oxidation of Cu(100).⁴¹

The above *ex situ* AFM observation indicate that the oxide growth involves the consumption of adjacent terrace atoms that results in pit formation on the terrace. To further conform this speculation, we can compare the volume of the oxide islands with the volume of the adjacent pits. From the surface profile in Figs. 7(a) and 7(b), oxide islands have a shallow profile which can be seen as a cone with high aspect ratio. The volume of the pits can be measured by the lateral area and vertical depth of the pits. The volume (V_i) of an oxide island can then be obtained through $V_i = \frac{1}{3} \pi s_i h_i$ by measuring the island height (h_i) and base area (s_i). Similarly, the volume (V_p) of the pits can be calculated through $V_p = s_p h_p$ by measuring the lateral area (s_p) and vertical depth (h_p) of the pits. Similarly, the volume (V_p) of the pits can be calculated through $V_p = s_p h_p$ by measuring the lateral area (s_p) and vertical depth (h_p) of the pits. The number of Cu atoms

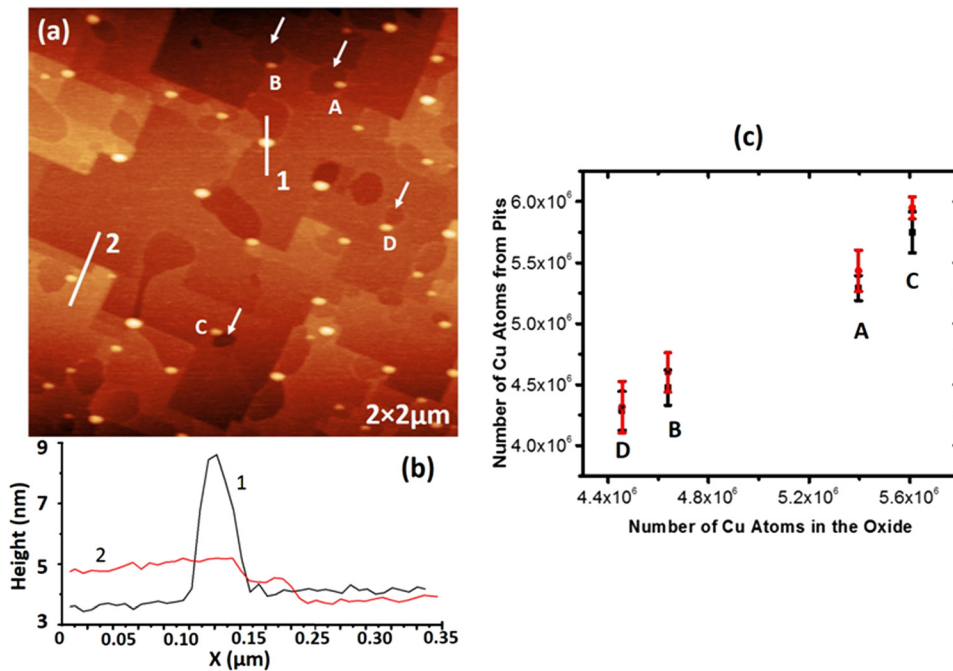


FIG. 7. (a) AFM height image of the Cu-5 at. %Pt(100) surface oxidized at 400 °C for 1 min; (b) surface profile of line 1 and 2 shown in (a); (c) number of Cu atoms depleted from the pits (red) vs. number of Cu atoms in the corresponding oxide islands (black), where A, B, C, and D represent the oxide islands indicated in (a).

in the oxide island (N_i) and the associated pit (N_p) can be determined from the calculated volumes V_i and V_p by $N_i = \frac{4V_i}{V_{\text{Cu}_2\text{O}}}$ and $N_p = \frac{4V_p}{V_{\text{Cu}}}$, where $V_{\text{Cu}_2\text{O}}$ and V_{Cu} are the unit cell volumes for Cu_2O and Cu, respectively. We found a perfect match between consumed Cu atoms from pits and the Cu atoms in the corresponding Cu_2O islands as illustrated in Fig. 7(c). To summarize, in the initial oxidation of the Cu-5 at. %Pt(100) surface, oxide islands can nucleate on the terrace region and Cu atoms on the terrace can then be expelled from the terrace for the oxide growth.

IV. CONCLUSION

Surface oxidation of the Cu-Pt(100) alloys has been investigated by *in situ* TEM visualization of the nucleation kinetics and morphological evolution of oxide islands at different oxidation temperatures. The oxidation proceeds via the nucleation and growth of oxide islands. At relatively low oxidation temperature (<400 °C), it is observed that the nucleation density of oxide islands and the oxide surface coverage can be promoted by alloying more Pt in the Cu-Pt alloys. The apparent nucleation activation energy for the oxidation of the Cu-5 at. %Pt(100) surface is determined as 0.3 ± 0.15 eV extracted from the Arrhenius dependence of the nucleation density on the oxidation temperature. At higher temperature (>400 °C), the oxide islands have more pronounced 3D growth resulting in sparsely distributed large oxide islands highly protruding above the alloy surface. Increasing the oxidation temperature above 700 °C results in the transition of the compact oxide islands to a dendritic growth morphology. While this dendritic morphology is similar as that on Cu-Au, the oxidation temperature required for such a dendritic shape transition is 100 °C higher for Cu-Pt, owing to the lower mobility of Pt in Cu. The *ex situ* AFM studies revealed that the oxide islands nucleate homogeneously across the alloy surface and the oxide growth consumes local terrace Cu atoms that results in the formation of surface pits. Since oxide islanding

during oxidation has been observed for many metals and alloys, these results may have broader implications in manipulating the oxidation of metals to affect the reaction product morphology and the oxidation kinetics.

ACKNOWLEDGMENTS

This research was supported by the U.S. Department of Energy, Office of Basic Energy Sciences, Division of Materials Sciences and Engineering under Award No. DE-FG02-09ER46600. The Cu-Pt thin film deposition and AFM experiments were conducted in the Nanofabrication and Characterization Facility at the Univ. of Pittsburgh. NSF Award No. 1200415 provided some support of the *in situ* UVH-TEM.

¹G. R. Wallwork, *Rep. Prog. Phys.* **39**, 401–485 (1976).

²J. Knudsen, A. U. Nilekar, R. T. Vang, J. Schnadt, E. L. Kunkes, J. A. Dumesic, M. Mavrikakis, and F. Besenbacher, *J. Am. Chem. Soc.* **129**, 6485–6490 (2007).

³N. Barrabes, J. Just, A. Dafinov, F. Medina, J. L. G. Fierro, J. E. Sueiras, P. Salagre, and Y. Cesteros, *Appl. Catal., B* **62**, 77–85 (2006).

⁴W. Guan, M. Liu, S. Long, Q. Liu, and W. Wang, *Appl. Phys. Lett.* **93**, 223506 (2008).

⁵W. A. Lanford, P. J. Ding, W. Wang, S. Hymes, and S. P. Murarka, *Mater. Chem. Phys.* **41**, 192–198 (1995).

⁶K. Mistry, C. Allen, C. Auth, B. Beattie, D. Bergstrom, M. Bost, M. Brazier, M. Buehler, A. Cappellani, R. Chau, C.-H. Choi, G. Ding, K. Fischer, T. Ghani, R. Grover, W. Han, D. Hanken, M. Hattendorf, J. He, J. Hicks, R. Huessner, D. Ingerly, P. Jain, R. James, L. Jong, S. Joshi, C. Kenyon, K. Kuhn, K. Lee, H. Liu, J. Maiz, B. McIntyre, P. Moon, J. Neiryneck, S. Pae, C. Parker, D. Parsons, C. Prasad, L. Pipes, M. Prince, P. Ranade, T. Reynolds, J. Sandford, L. Shifren, J. Sebastian, J. Seiple, D. Simon, S. Sivakumar, P. Smith, C. Thomas, T. Troeger, P. Vandervoorn, S. Williams, and K. Zawadzki, *Tech. Dig. -Int. Electron. Devices Meet.* **2007**, 247–250.

⁷P. H. Holloway, *J. Vac. Sci. Technol.* **18**, 653–659 (1981).

⁸P. H. Holloway and J. B. Hudson, *Surf. Sci.* **43**, 123–140 (1974).

⁹S. Aggarwal, A. P. Monga, S. R. Perusse, R. Ramesh, V. Ballarotto, E. D. Williams, B. R. Chalamala, Y. Wei, and R. H. Reuss, *Science* **287**, 2235–2237 (2000).

¹⁰K. R. Lawless, *Rep. Prog. Phys.* **37**, 231–316 (1974).

- ¹¹G. W. Zhou and J. C. Yang, *Appl. Surf. Sci.* **210**, 165–170 (2003).
- ¹²G. W. Zhou and J. C. Yang, *J. Mater. Res.* **20**, 1684–1694 (2005).
- ¹³M. Lampimaki, K. Lahtonen, M. Hirsimaki, and M. Valden, *J. Chem. Phys.* **126**, 034703 (2007).
- ¹⁴K. Lahtonen, M. Hirsimaki, M. Lampimaki, and M. Valden, *J. Chem. Phys.* **129**, 124703 (2008).
- ¹⁵P. H. Holloway and J. B. Hudson, *Surf. Sci.* **43**, 141–149 (1974).
- ¹⁶E. E. Hajcsar, P. R. Underhill, and W. W. Smeltzer, *Langmuir* **11**, 4862–4872 (1995).
- ¹⁷H. B. Groen and J. T. M. De Hosson, *Scr. Mater.* **38**, 769–773 (1998).
- ¹⁸J. T. M. De Hosson, H. B. Groen, B. J. Kooi, and V. Vitek, *Acta Mater.* **47**, 4077–4092 (1999).
- ¹⁹J. T. M. De Hosson and B. J. Kooi, *Surf. Interface Anal.* **31**, 637–658 (2001).
- ²⁰G. W. Zhou, L. Wang, R. C. Birtcher, P. M. Baldo, J. E. Pearson, J. C. Yang, and J. A. Eastman, *Phys. Rev. Lett.* **96**, 226108 (2006).
- ²¹G. W. Zhou, J. A. Eastman, R. C. Birtcher, P. M. Baldo, J. E. Pearson, L. J. Thompson, L. Wang, and J. C. Yang, *J. Appl. Phys.* **101**, 033521 (2007).
- ²²L. Wang, G. W. Zhou, J. A. Eastman, and J. C. Yang, *Surf. Sci.* **600**, 2372–2378 (2006).
- ²³L. L. Luo, Y. H. Kang, J. C. Yang, D. Su, E. A. Stach, and G. W. Zhou, *Appl. Phys. Lett.* **104**, 121601 (2014).
- ²⁴G. W. Zhou, W. Y. Dai, and J. C. Yang, *Phys. Rev. B* **77**, 245427 (2008).
- ²⁵G. W. Zhou and J. C. Yang, *Phys. Rev. Lett.* **93**, 226101 (2004).
- ²⁶L. L. Luo, Y. H. Kang, J. C. Yang, and G. W. Zhou, *Appl. Surf. Sci.* **259**, 791–798 (2012).
- ²⁷G. W. Zhou, *Phys. Rev. B* **81**, 195440 (2010).
- ²⁸L. L. Luo, Y. H. Kang, J. C. Yang, and G. W. Zhou, *J. Appl. Phys.* **111**, 083533 (2012).
- ²⁹M. Hirsimaki, M. Lampimaki, K. Lahtonen, I. Chorkendorff, and M. Valden, *Surf. Sci.* **583**, 157–165 (2005).
- ³⁰G. W. Zhou and J. C. Yang, *Phys. Rev. Lett.* **89**, 106101 (2002).
- ³¹J. Tersoff and R. M. Tromp, *Phys. Rev. Lett.* **70**, 2782–2785 (1993).
- ³²M. Alatalo, S. Jaatinen, P. Salo, and K. Laasonen, *Phys. Rev. B* **70**, 245417 (2004).
- ³³G. W. Zhou, L. L. Luo, L. Li, J. Ciston, E. A. Stach, and J. C. Yang, *Phys. Rev. Lett.* **109**, 235502 (2012).
- ³⁴T. Ogawa, A. Kuwabara, C. A. J. Fisher, H. Moriwake, and T. Miwa, *J. Phys. Chem. C* **117**, 9772–9778 (2013).
- ³⁵J. C. Yang, M. Yeadon, B. Kolasa, and J. M. Gibson, *Scr. Mater.* **38**, 1237–1241 (1998).
- ³⁶B. Hammer and J. K. Norskov, *Surf. Sci.* **343**, 211–220 (1995).
- ³⁷K. J. Andersson, F. Calle-Vallejo, J. Rossmeisl, and I. Chorkendorff, *J. Am. Chem. Soc.* **131**, 2404–2407 (2009).
- ³⁸G. W. Zhou and J. C. Yang, *Surf. Sci.* **531**, 359–367 (2003).
- ³⁹A. N. Aleshin, B. S. Bokstein, V. K. Egorov, and P. V. Kurkin, *Defect Diffus. Forum* **95–98**, 457–462 (1993).
- ⁴⁰A. N. Aleshin, V. K. Egorov, B. S. Bokstein, and P. V. Kurkin, *J. Appl. Phys.* **77**, 6239–6243 (1995).
- ⁴¹G. W. Zhou, L. L. Luo, L. Li, J. Ciston, E. A. Stach, W. A. Saidi, and J. C. Yang, *Chem. Commun.* **49**, 10862–10864 (2013).